Research paper

# Porous Co-MOF for cyanosilylation reaction and protective effect in child bronchial pneumonia by reducing the inflammatory response and IL-12 production in immune cells

Hongjun Yu, Heng Li, Qiang Zhang, Yue Shao, Yong-Ji Wang

*Department of Paediatrics, Affiliated Hospital of Changchun University of Chinese Medicine, Changchun 130021, China*

ABSTRACT

A new porous metal–organic framework (MOF) with the chemical formula of $[Co_2(FDDI)(H_2O)_3](DMA)_4$ (**1**, $H_4FDDI$ = 5,5′-(9H-fluorene-2,7-diyl) showing the **ttd**-type topological structure has been prepared by solvothermal method. The structural determination results reveal that the coordinated water molecule in the center of Co(II) has been able to be removed by activating **1** at 120 °C, resulting in a porous skeleton arranged by unsaturated Lewis acid Co(II) ions. That activated **1** has demonstrated a nice catalytic activity for the cyanosilylation of acetaldehydes using the $CH_2Cl_2$ as the solvent under mild conditions. Furthermore, the ELISA assay was performed to measure the content of IL-12 in macrophages after compound treatment. And the RT-PCR was conducted to reveal the activation of JAK/STAT signaling pathway after compound addition.

## 1. Introduction

As a common and frequently-occurring disease in pediatrics, bronchial pneumonia is defined as lung inflammation caused by various pathogenic pathogens, which can cause inflammatory pathological damage of multiple organs in the body [1,2]. With the development of detection technology, we gradually recognized the relationship between the immune system and in the body and the child bronchial pneumonia. During bronchial pneumonia infection, the pathogenic pathogens usually cause the dysfunction of the body's immune response, production of a variety of harmful cytokines, which are harmful for the body [3,4]. Besides, the insufficient immune system development in infants and young children may be the direct cause of the development of bronchial pneumonia. In patients with tracheal pneumonia, there is often combined with immune dysfunction in the body [5]. The recent researches showed that the changes in cytokines and serum cytokines such as IL-12 may be associated with the disease development.

The cyanosilylation of carbonyl compounds with TMSCN produces cyanohydrins, they are serviceable intermediates in the synthesis of many kinds of compounds, for example α-hydroxyacids, α-hydroxyketones as well as β-hydroxyamines, α-aminonitriles together with β-aminoalcohols, among many others [6–8]. Many different catalysts are quite active, lewis acids included. But beyond that, the $sp^2$ carbon of carbonyl group has been converted into $sp^3$ stereogenic center, so the

synthesis of asymmetric cyanohydrin has been widely studied. However, conversion together with enantioselectivity have been quite sensitive to substrate, catalyst as well as reaction conditions. The majority of homogeneous catalysts have been on the basis of privileged ligands such as chiral building blocks, which is usually working in concert with expensive metals of coordination [9,10].

Metal-organic framework (MOF) is a kind of solid material with permanent porosity together with crystallization. Because of its large specific surface area, permanent porosity, highly dispersed metal center as well as tunable chemical pore [11–14], it has recently shown great potential as adsorbents together with catalysts. Considering these properties, MOF has been further suited as a novel kind of candidate for homogeneous or heterogeneous catalysts. So far, various effective strategies have been reported, dominating MOFs structures on the basis of unsaturated metal centers. Nevertheless, the majority of this open metal sites in MOFs are only coordinated with one dissolvant. It leads to the degradation of catalytic performance. The development of a late-model type MOF, where the metal nodes with more than two coordinated solvents as an efficient catalytic center, and it has enormous potential in multiphase catalysis for their enhanced Lewis acidity [15–18]. Recent literatures have revealed some Co(II)-based MOFs show promising catalytic performance toward the cyanosilylation reaction and $CO_2$ chemical conversion for the strong Lewis acidity of the coordinated unsaturated $Co^{2+}$ centers. For instance, Zhang and co-workers developed a dynamic cobalt-MOF which could act as the

catalyst for the cyanosilylation reaction under the solvent-free conditions [19]. Chen et al have reported a porous MOF with Co6 clusters which behaves as the heterogeneous Lewis catalyst facilitates the chemical fixation of $CO_2$ coupling with epoxides into cyclic carbonates under mind conditions [20]. In this study, a microporous metal organic framework [$Co_2$(FDDI)($H_2O$)$_3$](DMA)$_4$ (**1**, $H_4$FDDI = 5,5′-(9H-fluorene-2,7-diyl)-diisocyanic acid with **ttd**-type topological structure has been synthesized by solvothermal method together with characterized. It is interesting to note that activation of **1** at 120 °C can remove the coordination water molecules in the Co(II) center and form a framework. There are unsaturated Lewis acid Co(II) ions in the pore. This activated **1** represent an excellent catalytic activity for the cyanosilylation of acetaldehydes using the $CH_2Cl_2$ as the solvent under mild conditions under mild conditions. In the biological research, we make further efforts to evaluate the protective function of complexes on child bronchial pneumonia treatment. This ELISA assay was performed to measure the content of IL-12, the results stated clearly that the chemical compound can be significantly reduced this production of inflammatory cytokines in macrophages. Besides, the RT-PCR was further conducted and the results revealed that the compound addition could inhibit the activation of JAK/STAT signaling pathway. In conclusion, the new compound was synthesized for the first time and its protective effect on child bronchial pneumonia was explored by reducing the inflammatory response and IL-12 production in immune cells.

## 2. Experimental

### 2.1. Chemicals and measurements

Raw materials, reagents together with solvents have been purchased from commercial sources as well as have been able to be applied without making further efforts to purify. The infrared spectra have been measured by Nicoletavatar 360 FT-IR spectrophotometer. This rmogravimetric analysis has been carried out in one nitrogen stream which is applying Q50 TGA (TA) thermal analysis equipment with a heating rate of 5 °C·min$^{-1}$. Powder X-ray diffraction patterns (PXRD) of that bulk samples have been measured on one MiniFlex (Cu Kα, λ = 1.5418 Å) under room temperature. GC analysis was carried out on an Agilent 7890B GC analyzer. Low-pressure (up to1 bar) gas adsorption isotherms ($N_2$) have been measured on ASAP 2020 specific surface area together with porosity analyzer.

### 2.2. Preparation and characterization for [$Co_2$(FDDI)](DMA)$_4$ (1)

The organic ligand $H_4$FDDI (0.06 mmol, 30 mg) as well as Co ($NO_3$)$_2$·6$H_2O$ (0.20 mmol) have been added to the DMF/anhydrous methanol (5 mL, v/4/1) mixed solution, together with then packaged in one small glass solution of 20 mL. In the bottle, cover it. The glass bottle has been placed in 353 K oven for forty-eight hours, then cooled to 298 K, then the light pink bulk crystal has been obtained. Then the complex **1** has been obtained by washing with DMF and MeOH three times. Elemental results for (**1**): C, 57.60; H, 4.04; N, 6.44%; C, 57.26; H, 3.99; N, 6.24%.

The X-ray data of compound **1** have been obtained through making use of Oxford Xcalibur E diffractometer. Utilizing this CrysAlisPro software for the sake of analyzing magnitude data together with convert these data. The original structural models of complexes **1** has been constructed through SHELXS procedure on this basis of the immediate approach together with corrected by utilizing SHELXL-2014 procedure on this basis of the least square approach. Mixing the whole non-Hydrogen atoms of complex **1** under anisotropic parameters together with the whole Hydrogen atoms have been fixed to their connected Carbon atoms geometrically through applying AFIX instructions. Table 1 represents numerical information as well as crystallographic parameters reorganized of compound **1**.

**Table 1**
Details and crystallographic parameters of complex **1**.

| Empirical equation | $C_{29}H_{20}Co_2O_{11}$ |
|---|---|
| Chemical formula weight | 662.31 |
| Temperature/K | 293(2) |
| Crystallized systems | monoclinic |
| Space group | $P2_1$ |
| a/Å | 9.9638(6) |
| b/Å | 17.024(5) |
| c/Å | 18.5358(6) |
| α/° | 90 |
| β/° | 94.962(3) |
| γ/° | 90 |
| Volume/Å$^3$ | 3132.3(9) |
| Z | 2 |
| $\rho_{calc}$g/cm$^3$ | 0.702 |
| μ/mm$^{-1}$ | 0.557 |
| Data/restraints/parameters | 12596/2/383 |
| Goodness-of-fit on F$^2$ | 0.967 |
| Final R indexes [I > =2σ (I)] | $R_1$ = 0.0597, ω$R_2$ = 0.1409 |
| Final R indexes [all data] | $R_1$ = 0.0966, ω$R_2$ = 0.1577 |
| Largest diff. peak/hole/e Å$^{-3}$ | 0.57/−0.41 |
| Flack parameter | 0.50(2) |
| CCDC | 1956688 |

### 2.3. ELISA assay of IL-12

After LPS stimulation and compound treatment, the IL-12 released into cell supernatant was detected by ELISA. This experiment was performed according to the protocols with some modifications. Briefly speaking, this macrophages in logarithmic growth stage have been seeded into six pore-plates at that final destiny of 1 × 10$^5$ cell/well, then the cell were placed and cultured in incubator with the temperature of 37 °C, 5% $CO_2$ condition for twelve hours to get 70–80% confluence. Next, 2 μg/mL LPS was added into cells for twelve hours stimulation, after completing the above operation then 5 μg/mL compound was added for further treatment. Subsequently, the cell supernatant was collected and the content of IL-12 was detected by ELISA assay. This experiment was repeated in triplicate.

### 2.4. RT-PCR detection

JAK/STAT signaling pathway is the upstream of the IL-12, which regulates the expression of the *il-12*. When finishing compound therapy, this relative expression of *jak* and *stat* was measured by RT-PCR. Briefly, the cells in this logarithmic growth stage have been seeded into six well-plates at the final destiny of 1 × 10$^5$ cell/well, and the 2 μg/mL LPS was added into cells for twelve hours stimulation, after completing the above operation then 5 μg/mL compound was exposure to cells for further therapy. After completing the above operation, these cells have been washed with PBS and the total RNA was collected with RNA extraction with manufacture's kit. Next, the RNA was quantified with spectrophotometer. The cDNAs was synthesized with cDNA Reverse Transcription Kit, followed by the RT-PCR preformation to test the relative expression of *jak* and *stat*, *gapdh* was used as an internal reference in this experiment. The relative expression level of *jak* and *stat* genes were calculated according to the $2^{-\Delta\Delta Ct}$ method. This experiment was repeated in triplicate.

## 3. Results & discussion

### 3.1. Crystallographic structure of complex 1

The targeted complex **1** could be afforded through reaction of Co ($NO_3$)$_2$·6$H_2O$ together with 5,5′-(9H-fluorene-2,7-diyl)-diisophthalic acid ligand in the mixed solvent of DMF/MeOH. It should be noted that the 5,5′-(9H-fluorene-2,7-diyl)-diisophthalic acid ligand could be
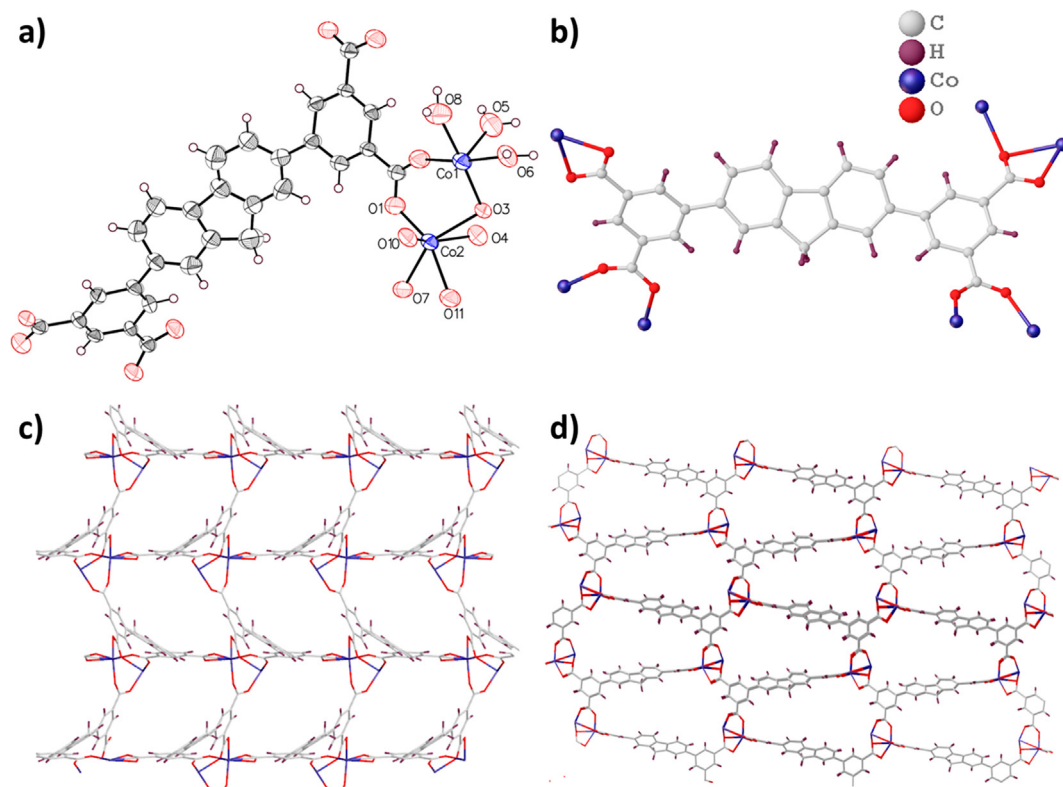
**Fig. 1.** (a) View for asymmetric unit for complex **1**. (b) From the perspective of coordination mode for this organic ligand (The inset shows the atom legends). (c) From the perspective of 3D framework of **1** showing this 1D channels from the [1 0 0] (d) and the [0 1 1] direction.
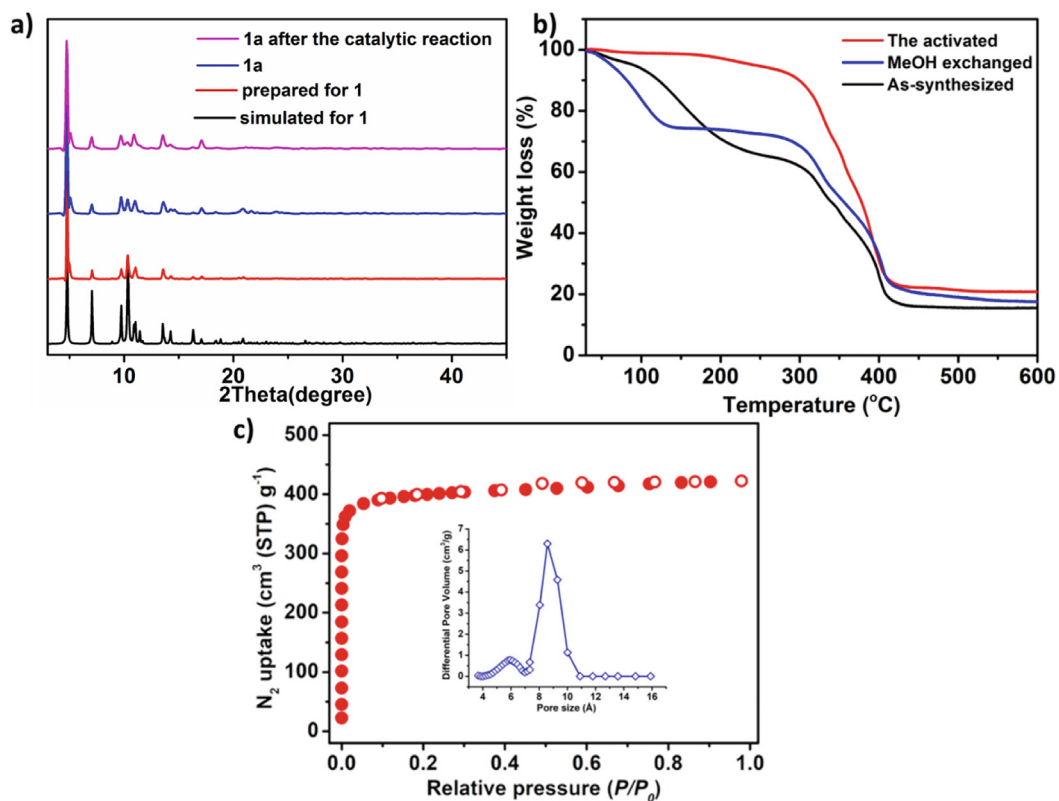


**Fig. 2.** (a) The PXRD pattern in **1**. (b) TGA curves of **1** as well as **1a**. (c) N$_2$ adsorption data of **1a**.

neither dissolved in MeOH nor water, and the addition of the DMF solvents could help to promote the solvothermal reaction. According to the crystal data collected at room temperature, the structure of complex **1** has been decomposed together with refined. These results state clearly that the prepared complex **1** crystallized in monoclinic space group $P2_1$ with cell parameters as follows: a = 9.9638(6) Å, b = 17.024(5) Å, c = 18.5358(6) Å, α = γ = 90°, β = 94.962°. The volume of this unit cell has been 3132.1(4) Å$^3$. This asymmetric unit of **1** has been made up of two crystallographic independent Co(II) ions, a complete deodorization FDDI$^{2-}$ligand together with three coordinated water molecules, All these contribute to the formation of one neutral framework. As shown in Fig. 1a, the Co(II) center is a distorted octahedron with one six-coordinated structure, in which the Co-O bond distance has been between 2.106 (4) and 2.216 (6) Å boundaries, which are comparable with those of the Co-MOFs based on the similar organic ligands [21,22]. As it is shown in Fig. 1b, a $Co^{2+}$ metal ion has been linked to six decarbonized carboxylic acid oxygen atoms from four carboxylic acids. The other is a decarboxylic acid coordinated by three water molecules together with three oxygen atoms from an independent FDDI$^{4-}$ ligand. As shown in Fig. 1c, two adjacent $Co^{2+}$ ions have been bridged by carboxylic acid to form a secondary construction unit (SBUs) of $Co_2(COO)_4$ connected to organic connectors to form a three-dimensional (4,4) connection network structure with **ttd**-type topology. As shown in Fig. 1c together with Fig. 1d, Co-MOF has three irregular rectangular channels. Considering the van der Waals radius, the diameter of the triangular channel along the axis is 14 × 6 Å$^2$. It is similar to rectangular as well as elliptical channels with aperture sizes of 4 × 8.4 Å$^2$ together with 7 × 5 Å$^2$, respectively, along the B together with C axes. According to PLATON analysis, the barrier-free traffic volume has been 2301 Å$^3$, accounting for 71.1% of the unit traffic volume of 3232.6 Å$^3$.

### 3.2. PXRD, TGA & BET analysis

In order to check the phase purity of the prepared complex **1**, the PXRD patterns for complex **1** were collected at room temperature by using the freshly prepared samples, and the results are shown in Fig. 2a. The calculated together with observed diffraction peaks have been in agreement with the purity of the sample. The difference of reflective intensity between simulated as well as observed results has been due to the different orientation of crystals in that powder samples. Thermal weightlessness analysis showed that the first weightlessness rate of four DMA molecules as well as three coordination water molecules has been 38.4% (calculated weightlessness rate has been 39.2%) in the temperature range of 25–232°. After dehydration, the skeleton has been stable below 362 °C, then decomposed after further heating. Inspired by its appropriate pore size as well as potential porosity, we encourage further exploration of the microporous properties of **1**. As it was shown in Fig. 2a, complex **1** has been evaluated for five hours at 313 K after the acetone has been fully exchanged, together with the desolvent or activated **1a** has been obtained. Obviously, the characteristic peaks of complex **1a** have been basically consistent with the simulated XRD spectra, as well as the microporous properties have been still dominant. After removing solvent molecules from the newly established framework, some displacements have been expected to be observed between **1a** and **1**. Furthermore, this TGA of activated **1** (**1a**) in the absence of two coordination water molecules, no weightlessness will occur below 180 °C, as well as it has been stable up to 342 °C. As it was shown in Fig. 2c, the $N_2$ adsorption isotherm of compound **1a** at 77 K reveals shows a type I adsorption isotherm, but there is no hysteresis desorption between the adsorptions. The adsorption quantity of N$^2$ at 77 K together with 1 atm achieved 412 cm$^3$/g (Fig. 2c). The estimated apparent Brunauer–Emmett–Teller (BET) surface area as well as Langmuir surface area of 1572 together with 1731 m$^2$/g, respectively. **1a** was analyzed by using the 77 K $N_2$ isotherm has been on the basis of the NLDFT model which shows the size distribution of narrow holes with centers at
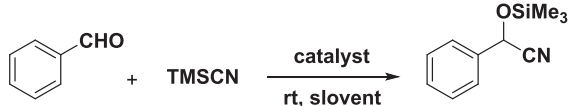
5.8 and 8.6 Å and they have been close to the size determined by the crystal structure.

### 3.3. Catalytic properties of 1a

In view of its large window size as well as high open metal density, we tested the activity of the synthesized framework **1** as a solid heterogeneous catalyst in the cyanidation of various aldehydes, i.e. using benzaldehyde as a model substrate, after completing the above operation then using the mixture of aldehyde together with trimethylsilyl cyanide for the cyanidation reaction, as well as a **1a** in CH$_2$Cl$_2$ at room temperature. As it was shown in Table 1, entry 1, with skeleton **1a** as catalyst (2 mol%), benzaldehyde has been highly converted to 2-[(trimethylsilyl) oxy] acetonitrile after ten hours in dichloromethane at room temperature. When the reaction time has been further extended to twenty-four hours, the yield of the product increased only slightly to 96%. In addition, no other else products have been tested, together with the yield of the product has been considered to be the conversion of benzaldehyde. With complex **1** as catalyst, the yield has been only 32% under the same conditions. The relationship between catalytic activity and structure is not clear in this study, however, the higher dialogue shown by compound **1a** than that shown by compound **1** may ultimately be related to the one-dimensional nanochannels in its accessible metal centers, as well as the Lewis acidity at the Co(II) site is also higher. As it was shown in Table 1, item 8, we measured the influence of the amount of catalyst at the same time, as well as solvent on the cyanation reaction catalyzed by **1a**. When the catalyst loading increased from 1.0 mol% to 2.0 mol%, as it was shown in Table 2, Item 6 & 7, the product yield increased from 75% to 94%. However, a further increase in load (up to 5%) only increased production by 1%. As it was shown in Table 2, we examined the catalytic reactions in different solvents at the same time, including MeCN, THF, CHCl$_3$, MeOH as well as CH$_2$Cl$_2$, in which CH$_2$Cl$_2$ (94% yield) has been the best solvent for the conversion, together with the worst solvent has been THF (63% yield) (Table 2, entry 7). In the absence of any catalyst, the blank test of 4-nitrobenzaldehyde has been carried out at room temperature. After ten hours of reaction, only 12% conversion has been tested. At the same time, the reactivity of Ni (NO$_3$)$_2$·6H$_2$O as well as free ligand (H$_3$L) in CH$_2$Cl$_2$ has been also tested. The yields have been 21% together with 16% respectively.

We also compared the activity of catalyst **1a** in the reaction of other

**Table 2**
Optimizing the cyanidation parameters of benzaldehyde with TMSCN together with**1a**.[a]



| Entry | Cat | Quant.[a] (mol%) | Time | Solvent | Conv.(%)[b] |
|-------|-----|------------------|------|---------|-------------|
| 1 | **1a** | 2 | 10 | CH$_2$Cl$_2$ | 94 |
| 2 | **1a** | 2 | 24 | CH$_2$Cl$_2$ | 96 |
| 3 | **1** | 2 | 10 | CH$_2$Cl$_2$ | 32 |
| 4 | **1a** | 1 | 10 | CH$_2$Cl$_2$ | 75 |
| 5 | **1a** | 5 | 10 | CH$_2$Cl$_2$ | 94 |
| 6 | **1a** | 2 | 10 | MeCN | 82 |
| 7 | **1a** | 2 | 10 | THF | 63 |
| 8 | **1a** | 2 | 10 | CH$_3$OH | 76 |
| 9 | – | – | 10 | CH$_2$Cl$_2$ | 12 |
| 10 | Ni(NO$_3$)$_3$·6H$_2$O | 2 | 12 | CH$_2$Cl$_2$ | 21 |
| 11 | H$_3$L | 2 | 12 | CH$_2$Cl$_2$ | 16 |

[a] Reaction conditions: 4-nitrobenzaldehyde (0.50 mmol), TMSCN (1.0 mmol), catalyst, together with solvent (2.0 mL) at room temperature.
[b] Calculated by GC–MS: mol(product)/mol(aldehyde) × 100.

**Table 3**
Catalytic cyanation of aldehydes in the presence of **1a**.



| Entry | $R_1$ | Time (h) | conversion[a] |
|-------|-------|----------|------------|
| 1 | Ph | 10 | 89% |
| 2 | $2\text{-}CH_3C_6H_4$ | 10 | 82% |
| 3 | $2\text{-}CH_3OC_6H_4$ | 10 | 77% |
| 4 | $3\text{-}NO_2C_6H_4$ | 10 | 93% |
| 5 | $3\text{-}ClC_6H_4$ | 10 | 91% |
| 6 | 1-naphth | 10 | 73% |
| 7 | 9-nathra | 10 | 32% |

[a] Conversion determined by GC.

substituted aromatic aldehydes with trimethylsilyl cyanide, together with produced corresponding cyanohydrin derivatives in 32–91% yield (Table 3). Aromatic aldehydes with strong electron-absorbing substituents (e.g. nitro together with chlorine) exhibit the highest reactivity (Table 3, items 4 together with 5), which may be related to the increase of electrophilicity of substrates. As expected, aldehydes containing electron-donating groups (for example methyl or methoxyl) exhibited lower yields (Table 3, items 2 together with 3). The yield of aromatic aldehydes with larger naphthalene rings is the lowest, which

may be due to their high molecular weight and inability to enter **1a** channel. In addition, to test framework stability of **1a** after the catalytic reaction, the catalyst **1a** was separated from the reaction system via the filtration and washed thoroughly using the MeOH, then its PXRD patterns were collected around room temperature. As shown in the Fig. 2a, a good comparability could be observed between the PXRD patterns of the as-prepared samples of 1a and those of the after the catalytic reaction, indicating its good framework stability in the catalytic process.

Based on the experimental results as well as previous reports, one reasonable reaction mechanism has been proposed to explain the process of cyanation catalyzed by **1a**. This unstable water molecules in compound **1a** channel have been removed by heating to expose them to unsaturated metal sites. Aldehydes have been activated by coordinated unsaturated Co (II) centers to react with TMSCN (Scheme 1). The product has been displaced by aldehyde, as well as the catalyst continues to activate aldehyde in next catalytic cycle.

### 3.4. Compound reduced the production of IL-12 in macrophages

The relationship between the immune system and in the body and the child bronchial pneumonia has been recognized recently years. During bronchial pneumonia infection, the pathogenic pathogens could cause the dysfunction of the body's immune response, leading to the production of a variety of harmful cytokines, such as IL-12, which is harmful for the body. Thus, in this experiment the IL-12 content was produced after that compound treatment. As it is showed in the results Fig. 3, this LPS stimulation could significantly increase the level of IL-12 in macrophages, which has been significantly different from that
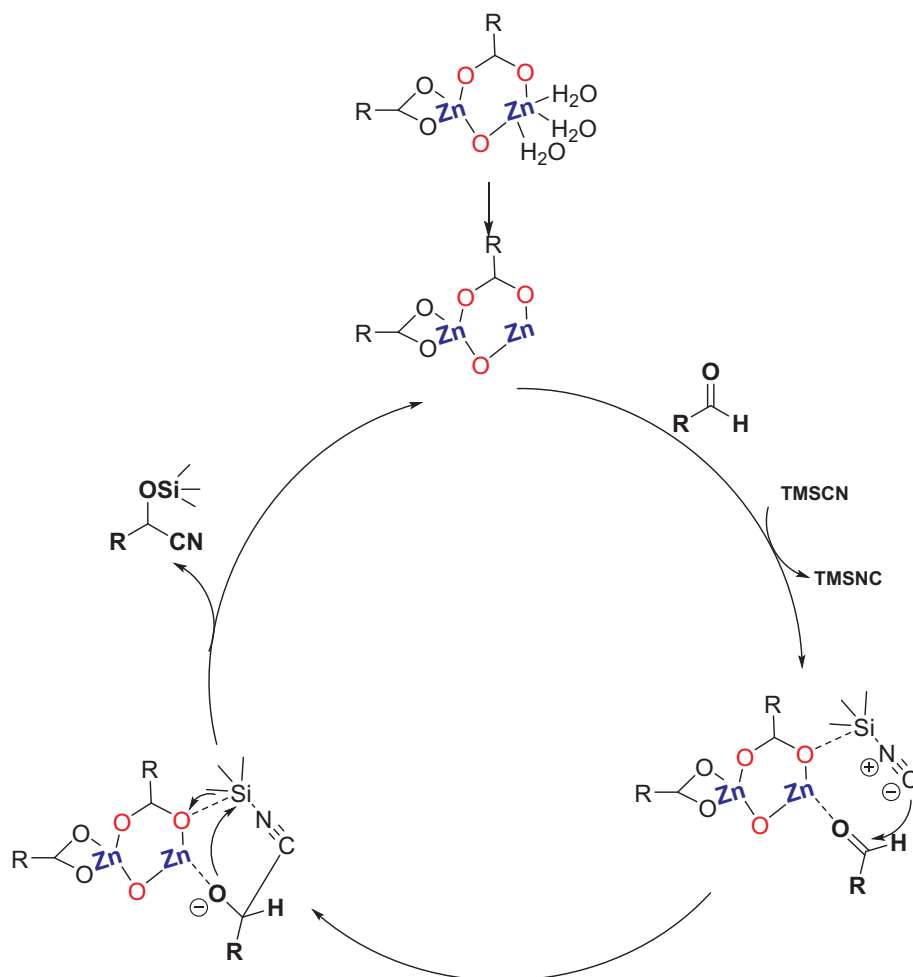


**Scheme 1.** The mechanism of cyanosilylation of carbonyl compounds catalyzed by **1a**.
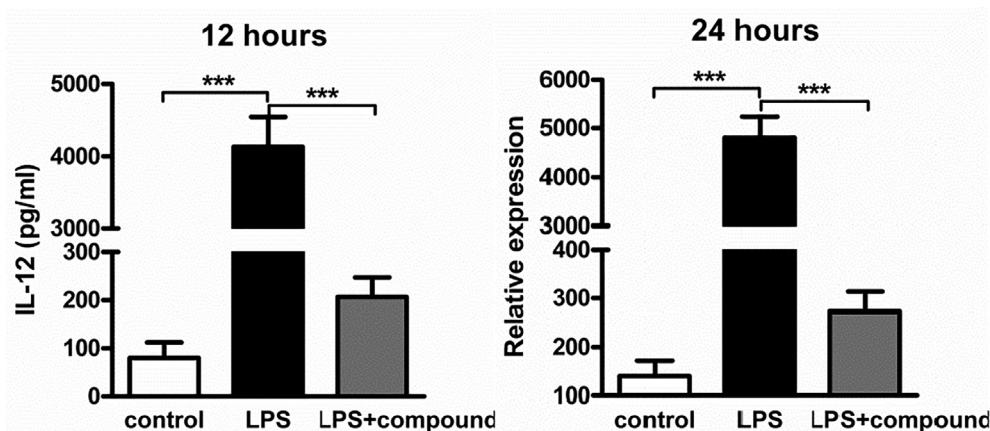
**Fig. 3.** Reduced IL-12 production in macrophages after compound treatment. The macrophages were stimulated with 2 μg/mL LPS was for 12 h stimulation, and incubated with 5 μg/mL compound for further treatment. The content of IL-12 in the cell supernatant was collected and detected by ELISA assay. *** means p < 0.005.

matched group. However, after that compound treatment, this production of IL-12 was obviously inhibited nearly to the level of the control group.

### 3.5. Compound inhibited the activation of JAK/STAT signal path in macrophages

JAK/STAT signaling pathway is the upstream of that IL-12, which regulates the expression of the *il-12*. So, the activation level of JAK/STAT signaling pathway after compound treatment has been detected by RT-PCR. From this outcome in Fig. 4, we can see the LPS pre-treatment significantly active the JAK/STAT signaling pathway, reflected as the up-regulated expression of *jak* and *stat* in macrophages. While, the up-regulated expression was obviously inhibited through adding chemical compound. This result indicated this chemical compound were able to inhibit this activity of JAK/STAT signal path in macrophages.

### 4. Conclusion

In conclusion, we have successfully prepared the micro-porous metal–organic skeleton which is having **ttd**-type topology structure. The interesting point of this work was that coordinated water molecules in Co(II) centers The activation of complex **1** at 120 °C to form a frame which were having a porous lining with unsaturated Lewis acidic Co(II) ions. That activated **1** has demonstrated a nice catalytic activity for the

cyanosilylation of acetaldehydes using the $CH_2Cl_2$ as the solvent under mild conditions. In the biological research, the compound with new structure was synthesized for the evaluation of the protective effect in child bronchial pneumonia. The ELISA assay of IL-12 indicated that the compound could significantly reduce the production of compound in macrophages. Besides, the RT-PCR further revealed that the compound addition could inhibit the activation of JAK/STAT signaling pathway. Finally, we synthesized the compound and revealed the protective effect of the compound in child bronchial pneumonia by reducing the inflammatory response and IL-12 production in immune cells

### 5. Data availability

The data used to support the findings of this study are included within the article.

### Author contributions

Hongjun Yu and Heng Li carried out the experiments, and wrote the manuscript.

Qiang Zhang and Yue Shao contributed to characterizations.

Yong-Ji Wang contributed to the experiments and writing related to biological activity study.
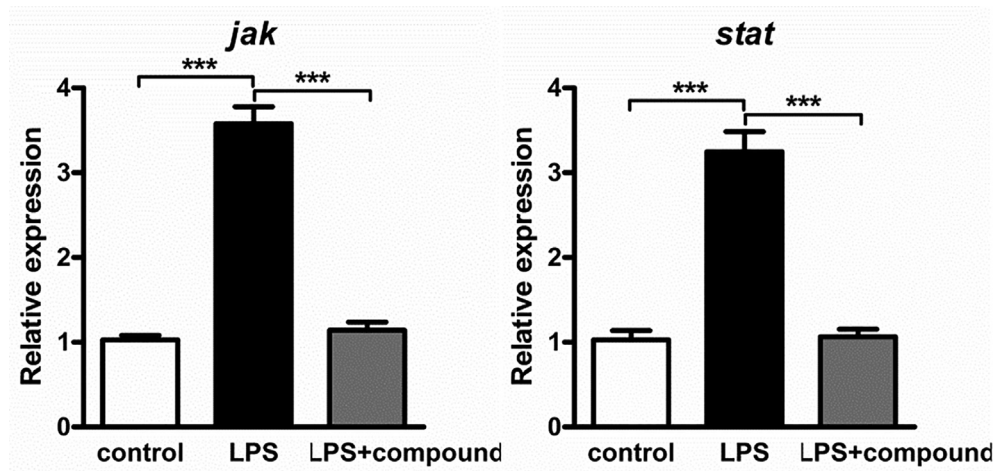


**Fig. 4.** Inhibited JAK/STAT signaling pathway activity in macrophages after compound treatment. The macrophages were stimulated with 2 μg/mL LPS was for 12 h stimulation, and incubated with 5 μg/mL compound for further treatment. The activation of JAK/STAT signal path in macrophages has been detected through RT-PCR. *** means p < 0.005.

## Conflicts of interest

The author(s) declare(s) that there is no conflict of interest regarding the publication of this paper.

## Acknowledgements

## Appendix A. Supplementary data

Supplementary data to this article can be found online at https://doi.org/10.1016/j.ica.2020.119426.

## References

[1] W. Chen, L. Chang, S.B. Ren, Z.C. He, G.B. Huang, X.H. Liu, Direct Z-scheme 1D/2D $WO_{2.72}/ZnIn_2S_4$ hybrid photocatalysts with highly-efficient visible-light-driven photodegradation towards tetracycline hydrochloride removal, J. Hazard. Mater. 384 (2020) 121308.

[2] J. Su, Z. Sheng, V.C.M. Leung, Y. Chen, Energy efficient tag identification algorithms for RFID: survey, motivation and new design, IEEE Wirel. Commun. 26 (2019) 118–124.

[3] J. Zhao, M. Xin, J. Zhang, Y. Sun, S. Luo, H. Wang, Y. Wang, X. Bi, Diclofenac inhibited the biological phosphorus removal: Performance and mechanism, Chemosphere 243 (2020) 125380.

[4] H. Wu, F. Chi, S. Zhang, J. Wen, J. Xiong, S. Hu, Control of pore chemistry in metal-organic frameworks for selective uranium extraction from seawater, Micropor. Mesopor. Mat. 288 (2019) 109567.

[5] V. Vitale, M. Sgorbini, V. Cuteri, S. Preziuso, A.R. Attili, F. Bonelli, cytological findings in bronchoalveolar lavage fluid of foals with pneumonia caused by Rhodococcus equi and other bacteria, J. Equine. Vet. Sci. 79 (2019) 9–12.

[6] V.K. Jakhar, M.K. Barman, S. Nembenna, Aluminum monohydride catalyzed selective hydroboration of carbonyl compounds, Org. Lett. 18 (2016) 4710–4713.

[7] B. Ullah, J. Chen, Z. Zhang, H. Xing, Q. Yang, Z. Bao, Q. Ren, 1-Ethyl-3-methylimidazolium acetate as a highly efficient organocatalyst for cyanosilylation of carbonyl compounds with trimethylsilyl cyanide, Sci. Rep. 7 (2017) 42699.

[8] M.K. Sharma, S. Sinhababu, G. Mukherjee, G. Rajaraman, S. Nagendran, A cationic aluminium complex: an efficient mononuclear main-group catalyst for the cyanosilylation of carbonyl compounds, Dalton T. 46 (2017) 7672–7676.

[9] A. Rostami, B. Atashkar, Synthesis, characterization and catalytic property of chiral oxo-vanadium ( + )-pseudoephedrine complex supported on magnetic nanoparticles $Fe_3O_4$ in the cyanosilylation of carbonyl compounds, Catal. Commun. 58 (2015) 80–84.

[10] A. Harinath, J. Bhattacharjee, H.P. Nayek, T.K. Panda, Alkali metal complexes as efficient catalysts for hydroboration and cyanosilylation of carbonyl compounds, Dalton T. 47 (2018) 12613–12622.

[11] X. Feng, X.L. Ling, L. Liu, L.Y. Wang, S.W. Ng, B.Y. Su, A series of 3D lanthanide frameworks constructed from aromatic multi-carboxylate ligand: Structural diversity, luminescence and magnetic properties, Dalton T. 42 (2013) 10292–10303.

[12] X. Feng, N. Guo, H.P. Chen, H.L. Wang, L.Y. Yue, X. Chen, S.W. Ng, X.F. Liu, L.F. Ma, L.Y. Wang, A series of anionic host coordination polymers, based on azoxybenzene carboxylate: structures, luminescence and magnetic properties, Dalton T. 46 (2017) 14192–14200.

[13] X. Feng, Y. Shang, H. Zhang, R. Li, W. Wang, D. Zhang, L. Wang, Z. Li, Enhance luminescence and tuning magnetic properties of lanthanide coordination polymers based on fluorine substituted and phenanthroline ligands, RSC Adv. 9 (2019) 16328–16338.

[14] X. Feng, Y.Q. Feng, N. Guo, Y.L. Sun, T. Zhang, L.F. Ma, L.Y. Wang, Series d − f heteronuclear metal − organic frameworks: color tunability and luminescent probe with switchable properties, Inorg. Chem. 56 (2017) 1713–1721.

[15] L.J. Zhang, C.Y. Han, Q.Q. Dang, Y.H. Wang, X.M. Zhang, Solvent-free heterogeneous catalysis for cyanosilylation in a modified sodalite-type Cu(II)-MOF, RSC Adv. 5 (2015) 24293–24298.

[16] J.J. Du, X. Zhang, X.P. Zhou, D. Li, Robust heterometallic MOF catalysts for the cyanosilylation of aldehydes, Inorg. Chem. Front. 5 (2018) 2772–2776.

[17] A. Bhunia, S. Dey, J.M. Moreno, U. Diaz, P. Concepcion, K. Van Hecke, C. Janiak, P. Van Der Voort, A homochiral vanadium-salen based cadmium Bpdc MOF with permanent porosity as an asymmetric catalyst in solvent-free cyanosilylation, Chem. Commun. 52 (2016) 1401–1404.

[18] F.Z. Jin, C.C. Zhao, H.C. Ma, G.J. Chen, Y.B. Dong, Homochiral BINAPDA-Zr-MOF for heterogeneous asymmetric cyanosilylation of aldehydes, Inorg. Chem. 58 (2019) 9253–9259.

[19] X. Cui, M.C. Xu, L.J. Zhang, R.X. Yao, X.M. Zhang, Solvent-free heterogeneous catalysis for cyanosilylation in a dynamic cobalt-MOF, Dalton T. 44 (2015) 12711–12716.

[20] D.M. Chen, X.J. Zhang, A polyhedron-based metal-organic framework with a rare hexanuclear Co(II) cluster for selective sorption and chemical conversion for $CO_2$, J. Solid State Chem. 278 (2019) 120906.

[21] X. Feng, Y.Q. Feng, J.J. Chen, S.W. Ng, L.Y. Wang, J.Z. Guo, Reticular three-dimensional 3d–4f frameworks constructed through substituted imidazole-dicarboxylate: syntheses, luminescence and magnetic properties study, Dalton T. 44 (2015) 804–816.

[22] X. Feng, J.L. Chen, R.F. Bai, L.Y. Wang, J.T. Wei, X.X. Chen, Two unique cobalt-organic frameworks based on substituted imidazole-dicarboxylate and dipyridyl-type ancillary ligands: Crystal structures and magnetic properties, Inorg. Chem. Commun. 66 (2016) 41–46.